Physical Existence of Relativistic Stellar Models within the context of Anisotropic Matter Distribution

M. Sharif[1,2*], Tayyab Naseer[1†] and Hira Shadab[1‡]
[1]Department of Mathematics and Statistics, The University of Lahore, 1-KM Defence Road Lahore-54000, Pakistan.
[2]Research Center of Astrophysics and Cosmology, Khazar University, Baku, AZ1096, 41 Mehseti Street, Azerbaijan.

Abstract

Two distinct non-singular interior models that describe anisotropic spherical configurations are presented in this work. We develop the Einstein field equations and the associated mass function in accordance with a static spherical spacetime. We then discuss certain requirements that must be satisfied for compact models to be physically validated. Two distinct limitations are taken into account to solve the field equations, including different forms of the radial geometric component and anisotropy, which ultimately leads to a couple of relativistic models. In both cases, solving the differential equations result in the appearance of integration constants. By equating the Schwarzschild exterior metric and spherical interior line element on the interface, these constants are explicitly obtained. The disappearance of the radial pressure on the hypersurface is also used in this context. We further use estimated radii and masses of six different stars to graphically visualize the physical properties of new solutions. Both of our models are deduced to be well-aligned with all physical

*msharif.math@pu.edu.pk
†tayyab.naseer@math.uol.edu.pk; tayyabnaseer48@yahoo.com
‡hirashadab123@gmail.com

requirements, indicating the superiority of the presence of anisotropy in compact stellar interiors over the perfect isotropic fluid content.

Keywords: Einstein's gravity; Relativistic models; Schwarzschild metric; Anisotropic fluid.
PACS: 04.20.Jb; 04.40.-b.; 04.40.Dg.

1 Introduction

The scientific community regards the general theory of relativity (GR) as the most accurate theory for understanding the nature of gravity. The Einstein field equations have been formulated using fundamental mathematical quantities, particularly the Einstein tensor and energy-momentum tensor (EMT), to provide a quantitative description of how matter influences spacetime structure. After the revolutionary work of Schwarzschild, the subject of finding the exact solution to equations related to a static sphere in GR and its extended frameworks has become a fascinating topic. He initially developed the external [1] and internal solutions [2] in 1916 by taking into account a sphere associated with the constant density. In order to describe physically feasible stellar objects, astrophysicists are now interested in finding the solutions of the gravitational equations that satisfy the necessary physical constraints. However, because of the non-linearity in the field equations, it might be challenging to find precise solutions that describe compact models. Recently, there has been progress in modeling the physically realistic stars that are associated to various fluid configurations and spacetime geometries.

In gravitational theories, the field equations are used to fully describe the structure of self-gravitating objects. These equations are difficult to solve because the higher derivatives of geometric components are involved. Depending on the situation, the solution may be analytic or numerical, and in the later scenario, initial and boundary conditions are required. Despite that, to get a comprehensive solution, more information about local physics is required. In the research of dense bodies, various recently identified elements revealed to affect the structural characteristics of such huge objects [3]-[7]. Finding a unique solution to the static anisotropic sphere without imposing constraints, like a well-established formulation of gravitational potentials, is impossible due to its three independent field equations with five unknowns (three matter variables and two metric functions). A well-behaved solution may be found by limiting the geometric coefficients, which lowers the number of unknowns. The Karmarkar condition, which provides a differential equation to derive one metric function in terms of another, has been used by many scholars [8]-[11]. The case of a disappearing Weyl tensor represents another key consideration in this framework [12].

Stars are the main constituents of our galaxy in the vast and captivating universe. Thermal reactions take place at the core of every star, and the outward pressure created by this response balances the object's gravitational attraction acting inward. Until the opposing forces are equal in magnitude, the star stays in an equilibrium state. When gravity takes over and the outward pressure drops, the stellar object undergoes gravitational collapse. A black hole, neutron star, or white dwarf might be the outcome of this phenomenon. It is interesting to note that this classification depends only on the initial mass of the star. The physical structure of these huge objects has captivated astronomers, who have focused on studying their evolution. Neutron stars, which are produced when large stellar masses collapse due to gravity, were the most interesting of all the other compact candidates. Their mass lies between 1-3 times that of our sun, and their dense core is composed of freshly generated neutrons. The star would not collapse again because of the pressure created by these neutrons, which resists the pull of gravity. Despite the fact that the concept of a neutron star initially came across in 1934 [13], a considerable time was spent for its demonstrative proof because these structures usually avoid from being directly detected because they emit insufficient radiation.

The ground breaking research of Jeans [14] revealed that several parameters controlling the internal geometry indicated the nature of fluid to be anisotropic in nature. Shortly after this, Lemaitre [15] introduced the initial anisotropic solution with unchanging density and pressure confined to radial and tangential components. Theoretically, Ruderman [16] found that huge star interiors (with densities more than $10^{15}g/cm^3$) might not have radial and tangential pressures to be equal. Numerous factors like the existence of pion condensation [17], powerful magnetic fields [18]-[21], nuclear forces [22], and superfluid region [23] etc. have been identified that produce anisotropy within a dense body. Initially, Bowers and Liang [24] examined how the anisotropy affected the stability of large objects and proposed that anisotropy should not be present in the core. They claimed that the equilibrium mass of the star and its surface redshift are significantly impacted by this factor. Numerous observations have been made in order to examine how anisotropy affects several characteristics of stellar models, including mass, radius, non-radial oscillation, and moment of inertia [25]-[29]. It was discovered that the magnitudes of the above described features directly correlate with that of the pressure anisotropy.

Lake [30] used the Newtonian equation to develop the corresponding anisotropic analog of the isotropic spherical spacetime. Herrera and Santos [31] investigated both Newtonian and relativistic fluids, and examined the potential causes of anisotropy in self-gravitating objects. They provided some relationships with the Weyl and shear tensors in order to better investigate its function. Herrera [32] used pressure anisotropy while studying relativistic fluid distributions. He demonstrated that during compact evolutionary phases, physical processes can lead to anisotropy, even if the fluid is initially isotropic. It is vital to highlight that any equilibrium configuration depicts the last phase of a dynamic process and there is no proof that anisotropy will vanish in the final state of equilibrium. Hence, even when starting from an isotropic pressure state, the end state configuration will theoretically display anisotropic pressure features. The presence of anisotropy inside giant stars is therefore not an exception, rather it necessarily exists. Numerous scholars have looked at how pressure anisotropy affects relativistic dense stats and have discovered results that are physically relevant [33]-cite40. Sharif and his associates [49, 50] creates anisotropic extensions of various isotropic spacetimes and explored the stability under particular parametric ranges.

The anisotropic solutions admitting spherical symmetry are developed in this research. The format of this paper is provided as follows. In the next section, we formulate the Einstein field equations assuming a spherical static spacetime associated with anisotropic matter content. A well-behaved solution must meet certain physical conditions which are listed in section **3**, so that we can analyze them for our novel solutions. In section **4**, we model a couple of anisotropic solutions using certain radial metric potentials and two anisotropies. The constants involved in metric components are obtained by applying the boundary conditions between the Schwarzschild exterior and the considered interior line elements. Additionally, a more-detailed graphical examination of the two constructed solutions is also given. The significance and implications of our results are finally presented in section **5**.

2 Static Sphere and Einstein Field Equations

The line element is an essential mathematical tool for expressing the internal spacetime of a celestial object. It is also important to understand the behavior of energy and matter inside these self-gravitating bodies. One of the primary advantages of the static spherical line element is the simplification of the field equations. In order to initiate our study, we suppose a spherical interior metric as

$$ds^2 = -\mathrm{A}_1^2 dt^2 + \mathrm{B}_1^2 dr^2 + r^2 d\Omega^2, \tag{1}$$

where $\mathrm{A}_1 = \mathrm{A}_1(r),\ \mathrm{B}_1 = \mathrm{B}_1(r)$ and $d\Omega^2 = d\theta^2 + \sin^2\theta d\phi^2$.

The Einstein-Hilbert action is the foundational principle that elegantly encodes the dynamics of spacetime curvature in relation to matter and energy. In the framework of classical field theory, physical laws are often derived by extremizing an action functional. For the gravitational theories, the action must satisfy two key requirements: *(i)* it should be invariant under arbitrary coordinate transformations, and *(ii)* it should be the simplest possible scalar invariant (the Ricci scalar R) involving the curvature of spacetime. The action functional, involving the matter Lagrangian density L_m, is defined as follows

$$I = \int \sqrt{-g}\left(\frac{R}{16\pi} + L_m\right) d^4x, \tag{2}$$

from which the Einstein field equations can be obtained using the variational principle as

$$G_{\alpha\eta} = 8\pi T_{\alpha\eta}, \tag{3}$$

where $G_{\alpha\eta} = R_{\alpha\eta} - \frac{1}{2}Rg_{\alpha\eta}$ with $R_{\alpha\eta}$, and $g_{\alpha\eta}$ being the Ricci tensor, and metric tensor, respectively. The geometrical structure is represented by $G_{\alpha\eta}$, also referred to the Einstein tensor. Moreover, the value on the right hand side, $T_{\alpha\eta}$, represents the usual matter source.

The anisotropic fluid interiors have attracted a lot of interest from scientists studying a variety of physical phenomena. Unlike perfect isotropic matter configuration where the physical factors remain the same in each direction, anisotropic fluid capture the crucial orientation-based variations in these quantities. This capability becomes significant particularly when analyzing systems exhibiting intrinsic directional symmetry, such as relativistic compact objects or extreme gravitational environments. Given our focus on anisotropic compact configurations, the EMT describing such an interior matter distribution is given by [51]-[53]

$$T_{\alpha\eta}=(p_t+\rho)\mathrm{U}_\alpha\mathrm{U}_\eta-p_t g_{\alpha\eta}-(p_t-p_r)\mathrm{V}_\alpha\mathrm{V}_\eta, \tag{4}$$

where $p_r,\ p_t,\ \rho,\ \mathrm{U}_\alpha$ and V_α represent the radial pressure, tangential pressure, energy density, four-velocity and four-vector, respectively. In the co-moving frame of reference, the final two physical terms become under the line element (1) as

$$\mathrm{U}_\alpha=(-\mathrm{A}_1,0,0,0),\quad \mathrm{V}_\alpha=(0,\mathrm{B}_1,0,0),$$

satisfying the following requirements

$$\mathrm{U}^\alpha\mathrm{U}_\alpha=-1,\quad \mathrm{V}^\alpha\mathrm{V}_\alpha=1,\quad \mathrm{U}^\alpha\mathrm{V}_\alpha=0.$$

The non-vanishing components of EMT (4) are

$$T_{00}=\rho\mathrm{A}_1^2,\quad T_{11}=p_r\mathrm{B}_1^2,\quad T_{22}=p_t r^2,\quad T_{33}=p_t r^2\sin^2\theta.$$

The independent components of the field equations (3) are determined under the spherical metric (1) and the fluid (4) as described below

$$8\pi\rho=-\frac{1}{r^2\mathrm{B}_1^2}+\frac{2\mathrm{B}_1'(r)}{r\mathrm{B}_1(r)^3}+\frac{1}{r^2}, \tag{5}$$

$$8\pi p_r=\frac{2\mathrm{A}_1'}{r\mathrm{A}_1\mathrm{B}_1^2}+\frac{1}{r^2\mathrm{B}_1^2}-\frac{1}{r^2}, \tag{6}$$

$$8\pi p_t=-\frac{\mathrm{A}_1'\mathrm{B}_1'}{\mathrm{A}_1\mathrm{B}_1^3}+\frac{\mathrm{A}_1'}{r\mathrm{A}_1\mathrm{B}_1^2}+\frac{\mathrm{A}_1''}{\mathrm{A}_1\mathrm{B}_1^2}-\frac{\mathrm{B}_1'}{r\mathrm{B}_1^3}, \tag{7}$$

where prime represents the derivatives with respect to r. In relativistic astrophysics, the mass function quantifies the gravitational mass enclosed within a given radius of a spherically symmetric spacetime, playing a key role in modeling compact objects. The expression for the Misner-Sharp mass $m(r)$ is [54]

$$m(r)=4\pi\int_0^r\rho r^2 dr\quad\Longrightarrow\quad m'(r)=4\pi r^2\rho(r). \tag{8}$$

The above differential equation can be resolved either numerically or analytically, depending on how complicated the expression for the energy density is. Equations (6) and (7) can be used to express the anisotropy of the system as

$$\Pi(r) = 8\pi(p_t - p_r) = -\frac{\mathrm{A}_1'\mathrm{B}_1'}{\mathrm{A}_1\mathrm{B}_1^3} + \frac{\mathrm{A}_1'}{r\mathrm{A}_1\mathrm{B}_1^2} + \frac{\mathrm{A}_1''}{\mathrm{A}_1\mathrm{B}_1^2} - \frac{\mathrm{B}_1'}{r\mathrm{B}_1^3}. \tag{9}$$

At the interior of the stellar configuration, $\Pi(r)$ should vanish, meaning that $p_r = p_t$ at that point. A positive anisotropic force induces repulsion that affect the stability by increasing pressure and density at the center. On the other hand, a negative force can cause contraction, decreasing pressure and density of the object.

3 Physical Acceptability Criteria for Relativistic Models

The Einstein gravitational equations that describe the interior composition of dense objects can be solved analytically or numerically using a variety of methods that have been proposed in the literature. Several authors compiled physically acceptable conditions, the fulfilment of which guarantees the physical viability of resulting model [55, 56]. In the following, we address these physical conditions.

- The presence of geometric singularities within the star is one of the basic components to be avoided. In order to verify that the metric potentials are not singular within a dense structure, we must examine the behavior of both time and radial functions mathematically as well as graphically. In a feasible self-gravitating interior, the behavior of these components should be finite in the core and positively rising outwards.

- The pattern of matter variables, including pressure components and energy density, should be positive and finite everywhere. Additionally, they have to attain their minimum (maximum) at $\Sigma : r = R$ $(r = 0)$. Similarly, it must be ensured that these variables will trend downward towards the boundary by checking if their first order derivatives vanish at $r = 0$ and become negative, otherwise.

- It should be noted that the existence of anisotropy, regardless of its sign, has a major impact on the self-gravitating stability of the model. An important factor in improving the stability of the star is its positive nature, which is defined by p_r being lower than p_t. This is explained by the pressure that is directed outward, which prevents the star from collapsing by acting as a supporting force that opposes gravity. On the other hand, the star may become unstable if there is negative anisotropy, in which p_r exceeds p_t since there is no outward directed pressure. Therefore, compared to a compact body having positive anisotropy, the stars admitting its negative profile are usually stable for less duration of time.

- The compactness, or mass-radius ratio, describes how firmly particles are bonded to one another in a self-gravitating system. The gravitational pull of extremely dense bodies, like neutron stars, is very strong. Its mathematical form is given as

$$\gamma(r) = \frac{m(r)}{r}. \tag{10}$$

In a spherical interior, its value must be < 0.44 everywhere [57]. Later research has shown that this limit can also be applied to anisotropic matter distributions, even though it was firstly suggested for an isotropic fluid sphere. Furthermore, a phenomenon, named the surface redshift, where light emitted from a massive object loses energy while escaping a strong gravitational field, causing its wavelength to stretch and shift toward red part of the spectrum. This happens because gravity drains energy from the light. The more intense the gravity, the more extreme the redshift will be. The amount of matter contained within a star and its compactness are used to determine the surface redshift. This is provided as

$$z(r) = \left(1 - \frac{2m}{r}\right)^{\frac{-1}{2}} - 1. \tag{11}$$

As the anisotropic matter content is under investigation in this analysis, at the surface, the redshift reaches its peak value by 5.211 in order to obtain an acceptable model [58].

- An expression for the equation of state is $p_j = \omega_j \rho$, where ω_j with $j = r, t$ stand for radial and transverse elements, respectively. They can be written as follows

$$\omega_r = \frac{p_r}{\rho}, \quad \omega_t = \frac{p_t}{\rho}. \tag{12}$$

A physically feasible fluid arrangement requires that the ratios of energy density to pressure components fall within a certain range of $[0, 1]$.

- Another essential element for confirming the accuracy of a stellar object are the energy conditions which are defined as the linear combinations of the fluid variables. To ensure that the dense object involves usual/ordinary fluid, they must be positive inside a star. For the current configuration, these energy conditions are

  $Null: \quad \rho + p_t \geq 0, \quad \rho + p_r \geq 0,$

  $Weak: \quad \rho + p_t \geq 0, \quad \rho + p_r \geq 0, \quad \rho \geq 0,$

  $Dominant: \quad \rho \pm p_t \geq 0, \quad \rho \pm p_r \geq 0,$

  $Strong: \quad \rho + p_r + 2p_t \geq 0, \quad \rho + p_t \geq 0, \quad \rho + p_r \geq 0,$

  $Trace: \quad \rho - p_r - 2p_t \geq 0.$

  As both pressures and density are positive, this ultimately results in positive weak, strong and null energy conditions, so we just need to study dominant and trace bounds.

- The hydrostatic equilibrium of the system is lost as a result of variations in the internal configuration caused by several components. Anisotropic, hydrostatic, and gravitational forces are the three candidates that are used to verify the equilibrium state of any compact model. According to the criterion of validity, the net sum of all the associated forces become null, mathematically represented by

$$f_g + f_h + f_a = 0. \tag{13}$$

  In the presence of anisotropy, the internal geometry of spherically symmetric dense celestial objects is expressed by the following evolution equation as [59, 60]

$$-\frac{\mathrm{M}_G}{r}(\rho + p_r)\frac{\mathrm{A}_1}{\mathrm{B}_1} - \frac{2}{r}(p_r - p_t) - p_r' = 0, \tag{14}$$

  where $\mathrm{M}_G(r)$ being the gravitational mass whose value is

$$\mathrm{M}_G(r) = \frac{r\mathrm{B}_1\mathrm{A}_1'}{\mathrm{A}_1^2}, \tag{15}$$

whose substitution in Eq.(14) yields

$$-\frac{\mathrm{A}_1'}{A_1}(\rho+p_r)-\frac{2}{r}(p_r-p_t)-p_r'=0. \tag{16}$$

The combination of Eqs.(13) and (16) results in different forces as

$$f_a = \frac{2}{r}(p_t-p_r), \tag{17}$$

$$f_h = -p_r', \tag{18}$$

$$f_g = -\frac{\mathrm{A}_1'}{\mathrm{A}_1}(\rho+p_r). \tag{19}$$

- Examining the structural stability of celestial systems has become a compelling subject in astrophysical studies. One of the various phenomena proposed in the literature is based on the speed of sound, with tangential and radial components given by $v_r^2=\frac{dp_r}{d\rho}$ and $v_t^2=\frac{dp_t}{d\rho}$, respectively. According to Abreu et al. [61], causality would be maintained in a system if the speed of light is greater than the speed of sound, i.e., $0<v_r^2,v_t^2<1$.

  Similarly, Herrera [62] suggested that cracking would take place in the internal fluid if a change in the sign of a radial force occurs during the evolution. To get a stable model, it must be avoided. He explained that the cracking would not occur only when $0<|v_t^2-v_r^2|<1$ holds.

  An important factor in determining the stability of compact stars is the adiabatic index, which is represented by Γ. The specific heat at constant volume divided by the specific heat at constant pressure is represented by this dimensionless parameter. This is also a measurement of the inner interaction and heat behavior of dense objects. Astrophysicists can learn more about the consistency requirements, pressure-density interactions, and general stability of the compact stellar objects by looking at this factor. The adiabatic index, in the case of anisotropic fluid, is expressed mathematically as

$$\Gamma_r=\frac{p_r+\rho}{p_r}\frac{dp_r}{d\rho}, \quad \Gamma_t=\frac{p_t+\rho}{p_t}\frac{dp_t}{d\rho}.$$

  Importantly, for a stable structure, the factors listed above must always be bigger than $\frac{4}{3}$ [63].

4 Novel Analytical Solutions under Anisotropic Fluid Source

Researchers have devised multiple analytical and numerical approaches to solve the Einstein field equations, motivated by persistent theoretical interest. We must now focus our efforts on overcoming this hurdle through a novel methodology. While various theoretical frameworks might resolve this problem, we direct our attention to two particularly insightful anisotropic factors along with g_{rr} metric functions. By selecting two different constraints, we balance the number of equations with the number of unknowns in the next subsections to find solutions of such non-linear differential equations.

4.1 Model I

After carefully examining various metric functions in the literature, researchers are encouraged to take into account known forms of the temporal and radial geometric terms. To continue our analysis, we thus select a specific g_{rr} metric potential which is provided as [64, 65]

$$\mathrm{B}_1^2(r) = \frac{a + 2br^2}{a + br^2}, \tag{20}$$

with a (dimensionless) and b (having dimension of $\frac{1}{\ell^2}$) being arbitrary constants. This particular metric, applied in the study of anisotropic interior compact models, maintains a finite and continuous behavior throughout. Moreover, $\mathrm{B}_1^2(r)|_{r=0} = 1$ and $\left(\mathrm{B}_1^2(r)\right)'|_{r=0} = 0$ ensure that the associated metric potential is both regular and singularity-free as shown in Figure **1**. By substituting the radial metric component (20) in Eq.(9), the following expression for anisotropy can be derived

$$\Pi(r) = \frac{-\left(a^2 + 4abr^2 + 2b^2r^4\right)\mathrm{A}_1' + r\left(a^2 + 3abr^2 + 2b^2r^4\right)\mathrm{A}_1'' + 2b^2r^3\mathrm{A}_1}{8\pi r \mathrm{A}_1\left(a + 2br^2\right)^2}, \tag{21}$$

which is a differential equation of second order. We modify the above equation as follows

$$\frac{\mathrm{A}_1''}{\mathrm{A}_1} - \frac{\mathrm{A}_1'}{\mathrm{A}_1}\left[\frac{a^2 + 4abr^2 + 2b^2r^4}{r\left(a^2 + 3abr^2 + 2b^2r^4\right)}\right] = \frac{r\Pi(r)\left(a + 2br^2\right)^2 - 2b^2r^3}{r\left(a^2 + 3abr^2 + 2b^2r^4\right)}. \tag{22}$$

We can solve Eq.(22) to find $\mathrm{A}_1(r)$ by specifying a unique expression of the factor $\Pi(r)$. We need to configure this element so that it effectively cancels out at the geometric center of astrophysical object. Moreover, the behavior of this quantity must exhibit a monotonically rising trend (i.e., $p_t > p_r$) with increasing radial distance to support the formation of stellar structures [33]. In this work, we select a form of anisotropy that meets this criteria and simplifies the process of solving the Eq.(22), given by

$$\Pi(r) = \frac{2b^2r^2}{(a+2br^2)^2}, \tag{23}$$

which leads Eq.(22) to

$$\frac{\mathrm{A}_1''}{\mathrm{A}_1} - \frac{\mathrm{A}_1'}{\mathrm{A}_1}\left[\frac{a^2+4abr^2+2b^2r^4}{r\left(a^2+3abr^2+2b^2r^4\right)}\right] = 0. \tag{24}$$

The solution of Eq.(24) is

$$\mathrm{A}_1 = \frac{C_1\left\{4\mathrm{f}_1 - \sqrt{2}a\ln\left(2\sqrt{2}\mathrm{f}_1 + \mathrm{f}_2\right)\right\}}{8b} + C_2, \tag{25}$$

where $\mathrm{f}_1 = \sqrt{a+br^2}\sqrt{a+2br^2}$ and $f_2 = 3a + 4br^2$. The constants C_1 and C_2 will be calculated later. We note that the given metric function exhibits regular behavior, as it fulfills the condition of being a constant at $r = 0$ and $\left(\mathrm{A}_1^2(r)\right)'|_{r=0} = 0$. Its physically suitable nature is further demonstrated in Figure **1**. Consequently, the matter components (ρ, p_r, p_t), based on the specific forms of the metric functions (20) and (25), are expressed as follows

$$8\pi\rho = \frac{b(3a+2br^2)}{(a+2br^2)^2}, \tag{26}$$

$$8\pi p_r = \frac{16bC_1\sqrt{a+br^2}}{\sqrt{a+2br^2}(C_1(4\mathrm{f}_1 - \sqrt{2}a\ln(2\sqrt{2}\mathrm{f}_1+\mathrm{f}_2)) + 8bC_2)} - \frac{b}{a+2br^2}, \tag{27}$$

$$\begin{aligned}8\pi p_t = {} & \frac{b}{\mathrm{f}_1^{5/2}(2\sqrt{2}\mathrm{f}_1 + (\mathrm{f}_2{}^2))(C_1(4\mathrm{f}_1 - \sqrt{2}a\ln(2\sqrt{2}\mathrm{f}_1+\mathrm{f}_2)) + 8bC_2)} \\ & \times \big[C_1\{a^2(24a^3 + a^2(17\sqrt{2}\mathrm{f}_1 + 104br^2) + 32b^2r^4(\sqrt{2}\mathrm{f}_1 + 2br^2)(48abr^2 \\ & \times (\sqrt{2}\mathrm{f}_1 + 3br^2))\ln(2\sqrt{2}\mathrm{f}_1 + \mathrm{f}_2 + 4(3a^3 + 17a^2br^2 + 30ab^2r^4 + 16b^3r^6)) \\ & \times ((17a^2 + 12a(\sqrt{2}\mathrm{f}_1 + 4br^2)16br^2(\sqrt{2}\mathrm{f}_1 + 2br^2))))\} - 8abC_2\{12\sqrt{2}a^3\end{aligned}$$

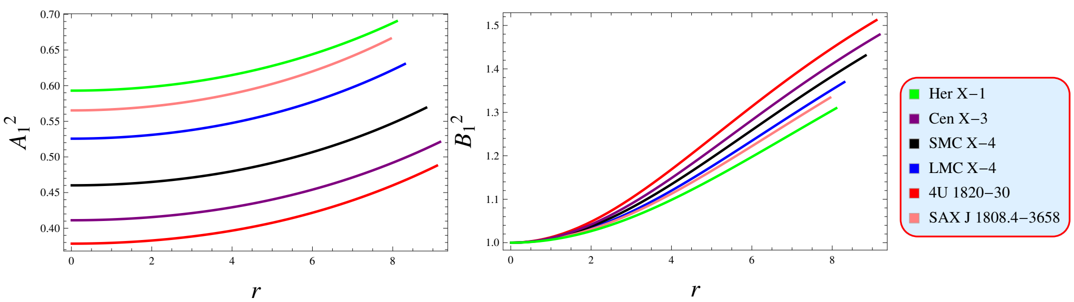

Figure 1: Temporal (25) and radial (20) metric functions for $b = 0.02$ corresponding to model I.

$$+\,a^2(17\mathrm{f}_1 + 52\sqrt{2}br^2) + 32b^2r^4\mathrm{f}_1 + \sqrt{2}br^2\} + 24abr^2(2\mathrm{f}_1 + 3\sqrt{2}br^2)\big]. \tag{28}$$

The matching conditions governing field behavior and their differential properties across matter interfaces or spatial boundaries play a fundamental role in compact star's modeling. These requirements, including metric continuity and curvature matching, guarantee smooth spacetime transitions and maintain field equations' validity. The Schwarzschild exterior metric represents a distinctive solution to the gravitational field equations for a static, spherically symmetric spacetime within the context of a vacuum. Therefore, this is the appropriate line element describing the outer geometry, expressed as

$$ds^2 = -\left(1 - \frac{2\mathrm{M}}{r}\right)dt^2 + \left(1 - \frac{2\mathrm{M}}{r}\right)^{-1}dr^2 + r^2 d\Omega^2. \tag{29}$$

Here, the total mass of the exterior region is denoted by M, with the condition that $r > 2\mathrm{M}$. In model I, the constants (a, C_1, C_2) are already introduced which can be calculated using matching conditions. They ensure continuous differentiability of curvature tensors (both intrinsic and extrinsic) at the boundary $(\Sigma : r = R)$.

The first fundamental form enforces continuity in the temporal and radial components of the metric, specifically, g_{tt} and g_{rr} for the metrics (1) and (29). This leads to

$$\mathrm{A}_1^2(R) = 1 - \frac{2\mathrm{M}}{R}, \tag{30}$$

$$\mathrm{B}_1^2(R) = \left(1 - \frac{2\mathrm{M}}{R}\right)^{-1}, \tag{31}$$

Table 1: Masses and radii of six different stars.

Stars	**Mass** ($M_\odot$)	**Radius (km)**
HerX − 1	0.85	8.1
CenX − 3	1.49	9.178
SMCX − 4	1.29	8.83
LMCX − 4	1.04	8.301
4U1820 − 30	1.58	9.1
SAXJ1808.4 − 3658	0.9	7.951

which yield after joining with Eqs.(20) and (25) as follows

$$\frac{C_1\left\{4\mathrm{f}_1^*-\sqrt{2}a\ln\left(2\sqrt{2}\mathrm{f}_1^*+\mathrm{f}_2^*\right)\right\}}{8b}+C_2 = \sqrt{1-\frac{2\mathrm{M}}{R}}, \tag{32}$$

$$\frac{a+bR^2}{a+2bR^2} = 1-\frac{2\mathrm{M}}{R}, \tag{33}$$

where $\mathrm{f}_1^*=\mathrm{f}_1(R)$ and $\mathrm{f}_2^*=\mathrm{f}_2(R)$. Equations (32) and (33) involve three unknown variables, necessitating an additional constraint for a unique solution. It is widely recognized in existing studies that the radial pressure vanishes at a certain finite r, which corresponds to the boundary of the star, denoted here by R. This condition, when coupled with Eq.(27), gives

$$p_r(R)=\frac{16C_1\sqrt{a+bR^2}}{\sqrt{a+2bR^2}(C_1(4\mathrm{f}_1^*-\sqrt{2}a\ln(2\sqrt{2}\mathrm{f}_1^*+\mathrm{f}_2^*))+8bC_2)}-\frac{1}{a+2bR^2}=0. \tag{34}$$

After combining Eqs.(32)-(34), the following constants are obtained as

$$a=\frac{bR^3-4b\mathrm{M}R^2}{2\mathrm{M}}, \tag{35}$$

$$C_1=\frac{b}{\mathrm{f}_1^*}\sqrt{1-\frac{2\mathrm{M}}{R}}, \tag{36}$$

$$C_2=\frac{1}{16}\sqrt{1-\frac{2\mathrm{M}}{R}}\left(\frac{\sqrt{2}a\ln\left(2\sqrt{2}\mathrm{f}_1^*+\mathrm{f}_2^*\right)}{\mathrm{f}_1^*}+12\right). \tag{37}$$

We use the predicted radii and masses from various star models, as shown in Table **1**, to examine the physical behavior of the resulting solutions. It is observed that both energy density and pressure attain their highest values at the center of the resulting configuration (Figure **2**). At the surface,

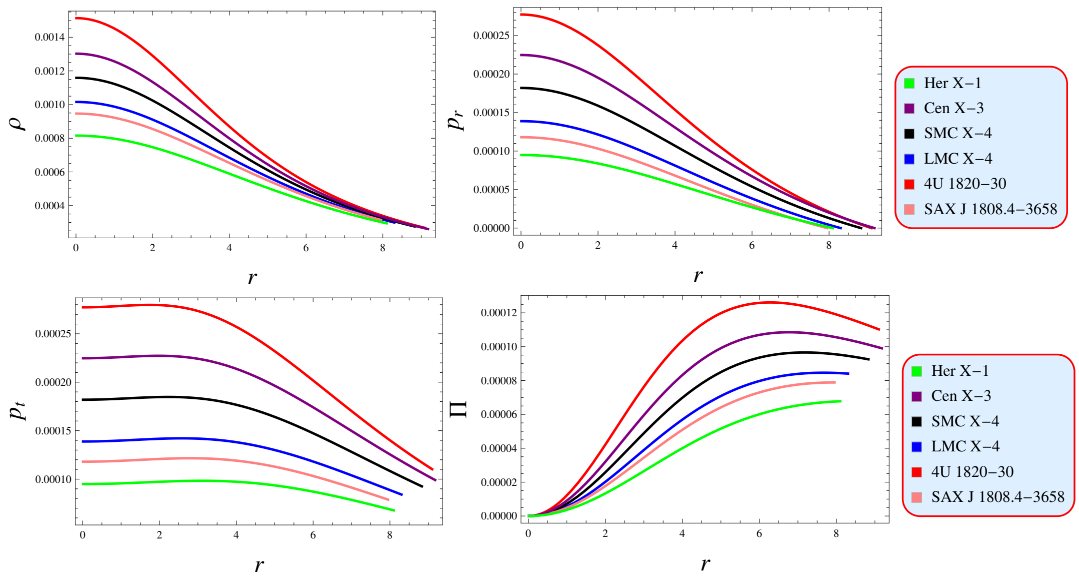

Figure 2: Fluid parameters for $b = 0.02$ corresponding to model I.

Table 2: Various physical factors for different stars corresponding to model I.

Stars	ρ_c**(gm/cm^3)**	ρ_s**(gm/cm^3)**	p_c**(dyne/cm^2)**
$\mathrm{HerX-1}$	1.0910×10^{15}	3.8583×10^{14}	1.1402×10^{35}
$\mathrm{CenX-3}$	1.7312×10^{15}	3.4262×10^{14}	2.6813×10^{35}
$\mathrm{SMCX-4}$	1.5412×10^{15}	3.6242×10^{14}	2.1788×10^{35}
$\mathrm{LMCX-4}$	1.3525×10^{15}	3.9212×10^{14}	1.6629×10^{35}
$\mathrm{4U1820-30}$	2.0175×10^{15}	3.5065×10^{14}	3.3319×10^{35}
$\mathrm{SAXJ1808.4-3658}$	6.5755×10^{15}	4.1968×10^{14}	1.4128×10^{35}

the pressure component in the radial direction nullifies, while at the core, both pressures are equal, (i.e., $p_t(0) = p_r(0)$), resulting in zero anisotropy at that point (as shown in the lower right panel). Additionally, the anisotropy increases with radius, supporting the stability and construction of dense stellar structures. Table **2** presents the corresponding analytical values of these quantities on the basis of which we can claim that our model I supports the existence of ultra-dense stellar configuration. Further, Figure **3** confirms the regular nature of the matter profiles by illustrating the required behavior of their first and second derivatives, mathematically, given by $\frac{d\rho}{dr}|_{r=0} = 0 = \frac{dp_r}{dr}|_{r=0} = \frac{dp_t}{dr}|_{r=0}$ and $\frac{d^2\rho}{dr^2}|_{r=0} < 0$, $\frac{d^2p_r}{dr^2}|_{r=0} < 0$, $\frac{d^2p_t}{dr^2}|_{r=0} < 0$.

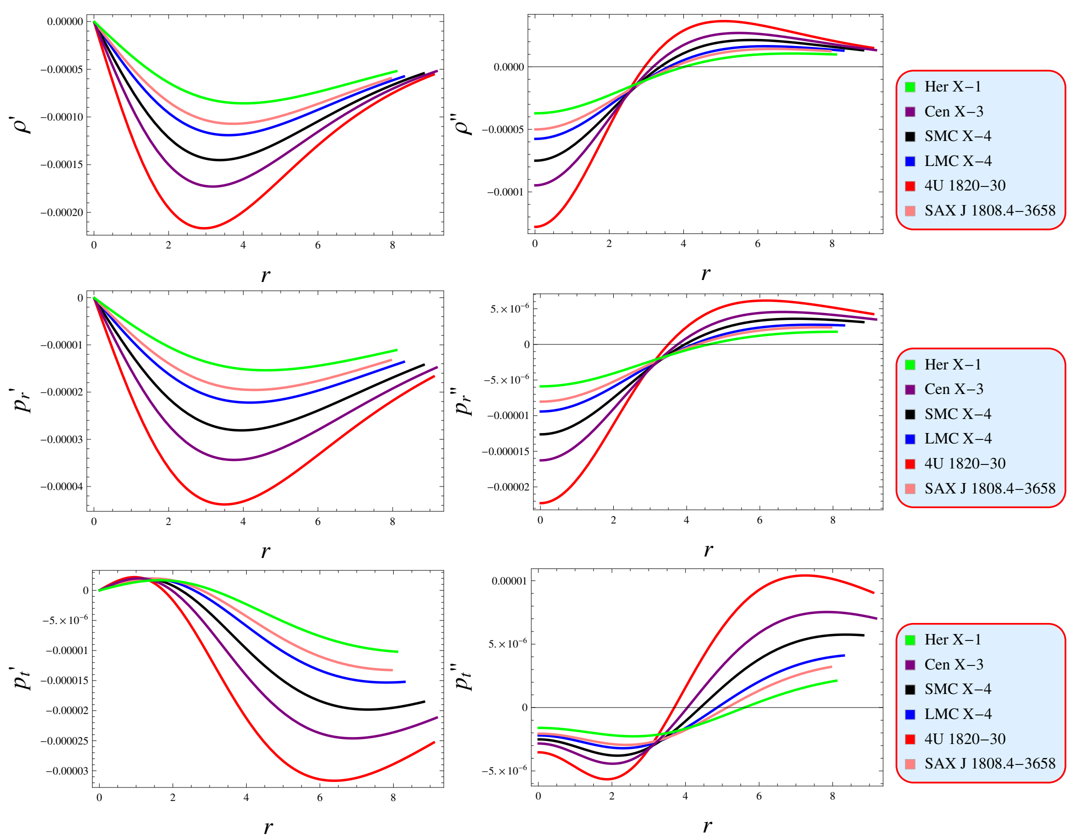

Figure 3: Regularity conditions for $b = 0.02$ corresponding to model I.

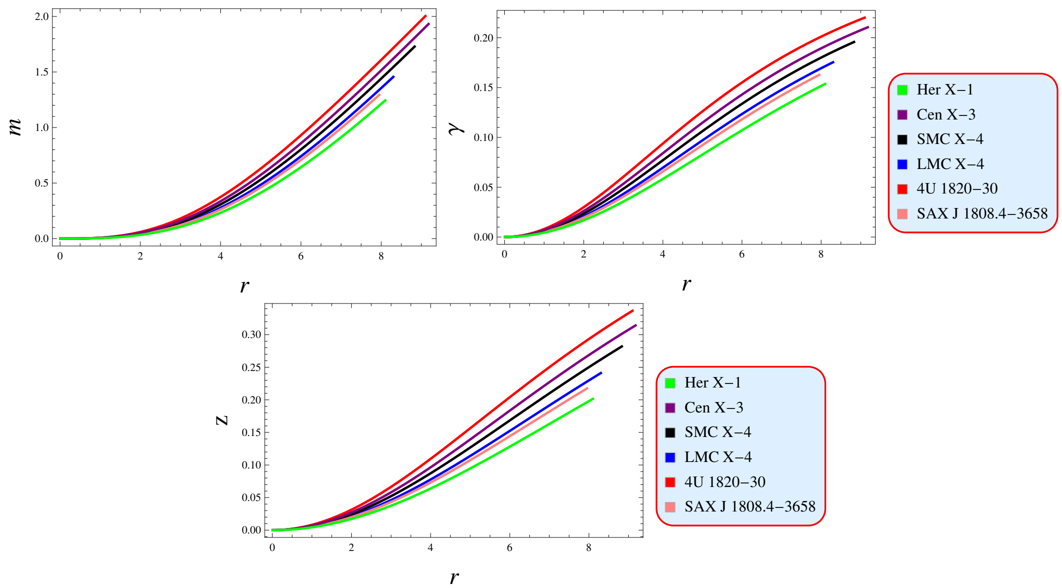

Figure 4: Physical factors for $b = 0.02$ corresponding to model I.

A continuous growing pattern of mass function is displayed in Figure **4** (top left). The compactness and redshift in the other two graphs similarly exhibit the behavior consistent with the observed data. Figure **5** depicts the behavior of equation of state parameters, and shows feasibility. Thus, the obtained solution is proved to be physically acceptable for stellar objects under investigation. Figure **6** shows trace and dominant energy conditions, with positive behavior everywhere in $0 < r < R$. As a result, our solution admits physical viability and contains the ordinary fluid in the interior distribution. The fundamental forces are graphically checked in Figure **7** (top left), and we find their net sum to be zero, claiming our model in the equilibrium state for all compact stars. Further, using the cracking and sound speed criteria, we examine the stability in the same Figure, and it is confirmed that our model I is stable. The stability conditions demonstrated in Figure **8** receive an additional validation of our model stability through the analysis of an adiabatic index.

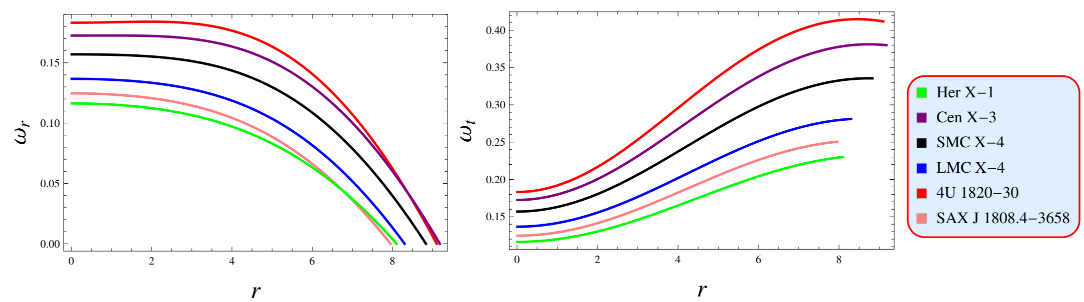

Figure 5: Equation of state parameters for $b = 0.02$ corresponding to model I.

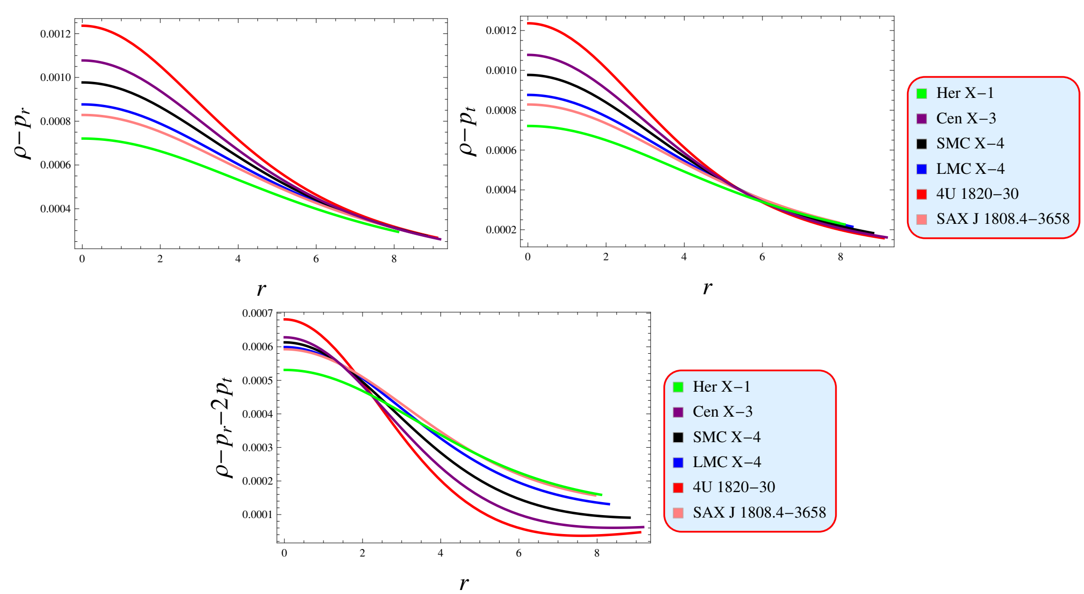

Figure 6: Energy bounds for $b = 0.02$ corresponding to model I.

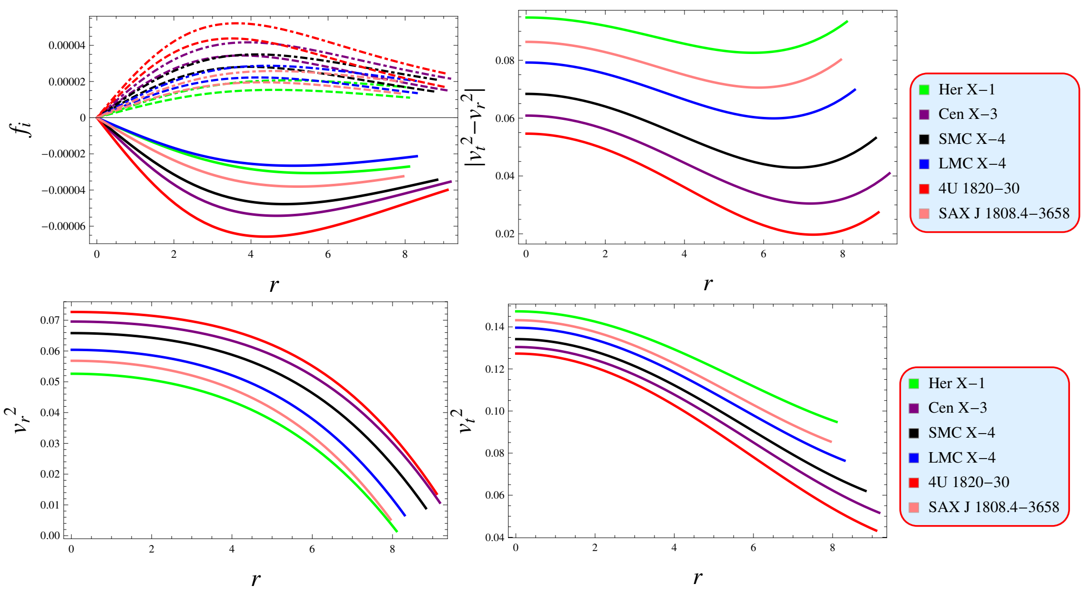

Figure 7: Equilibrium of forces, cracking, and sound speeds for $b = 0.02$ corresponding to model I.

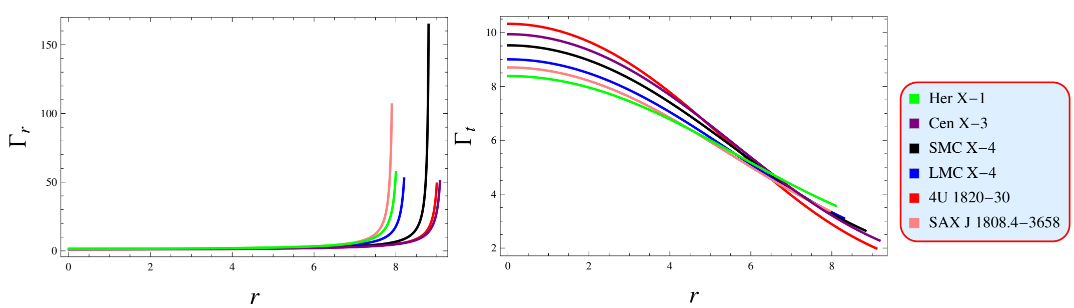

Figure 8: Adiabatic index for $b = 0.02$ corresponding to model I.

4.2 Model II

Here, we employ a different additional restriction to determine the analytic solution of the field equations in order to determine whether or not the related results assist in modeling a compact structure that is physically worthwhile. We take into account the anisotropic factor and a specific g_{rr} function in the preceding analysis. The later term is expressed as [59]

$$\mathrm{B}_1^2(r) = \frac{x(2r^2+y)}{(x-r^2)(r^2+y)}, \tag{38}$$

where x and y are two arbitrary constants having the dimension of ℓ^2. The anisotropic factor (9), after substituting Eq.(38), becomes

$$\Pi(r) = \frac{1}{8\pi r x \mathrm{A}_0(r)(2\mathrm{h}_2)^2}\big[r^3\mathrm{A}_0(r)(2x+y) - \mathrm{A}_0'(r)\{r^4(2x-y) + 4r^2xy + xy^2\} - r(\mathrm{h}_1)(2r^4+3r^2y+y^2)\mathrm{A}_0''(r)\big], \tag{39}$$

which is again a differential equation of the second order. Rearranging the equation given above results in

$$\frac{\mathrm{A}_1''}{\mathrm{A}_1} + \frac{\mathrm{A}_1'}{\mathrm{A}_1}\left[\frac{r^4(2x-y)+4r^2xy+xy^2}{r(r^2-x)(2r^4+3r^2y+y^2)}\right] = \frac{r\Pi(r)\big(2r^2+y^2\big) - r^3(2x+y)}{r\big(r^2-x\big)(2r^4+3r^2y+y^2\big)}. \tag{40}$$

One can find the solution of Eq.(40) if a specific form for the $\Pi(r)$ is provided. We already discussed the criteria for the anisotropic factor under which the resulting solution represents a physically valid dense structure. Following this, the anisotropic form that fulfills that criteria and facilitates us in analytically solving Eq.(40) is

$$\Pi(r) = \frac{r^2(2x+y)}{2r^2+y^2}, \tag{41}$$

which leads Eq.(40) to

$$\frac{\mathrm{A}_1''}{\mathrm{A}_1} + \frac{\mathrm{A}_1'}{\mathrm{A}_1}\left[\frac{r^4(2x-y)+4r^2xy+xy^2}{r(r^2-x)(2r^4+3r^2y+y^2)}\right] = 0, \tag{42}$$

through which A_1 is analytically determined by

$$\mathrm{A}_1 = \frac{D_1\sqrt{\frac{\mathrm{h}_1}{\mathrm{h}_2}}\{\sqrt{\mathrm{h}_2}(2r^2+y)\sqrt{\frac{\mathrm{h}_1}{\mathrm{h}_2}} + \sqrt{y}\mathrm{h}_2\sqrt{\frac{2r^2+y}{\mathrm{h}_2}}\mathrm{h}_3\}}{\sqrt{\mathrm{h}_1(2r^2+y)}} + D_2, \tag{43}$$

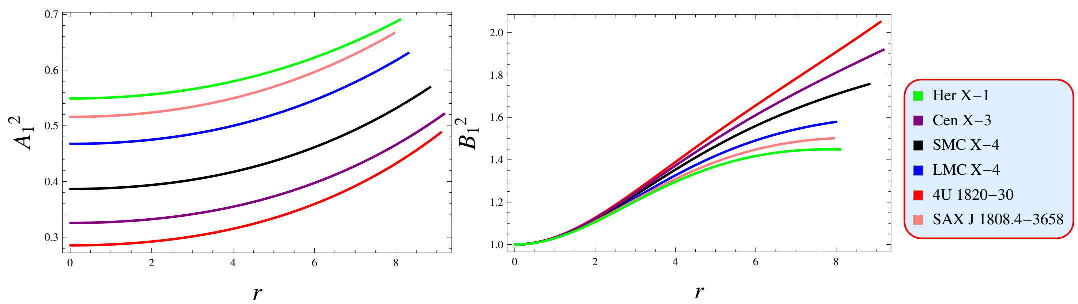

Figure 9: Temporal (43) and radial (38) metric functions for $y = 30$ corresponding to model II.

where $\mathrm{h}_1 = r^2 - x$, $\mathrm{h}_2 = r^2 + y$, and $\mathrm{h}_3 = \mathrm{E}\{\sin^{-1}(\frac{\sqrt{y}}{\sqrt{2}\sqrt{r^2+y}})|\frac{2(x+y)}{y}\}$. The regularity conditions require $\mathrm{A}_1^2(r)|_{r=0}$ to give a finite constant at $r = 0$, while its first derivative must vanish at the origin to guarantee a non-singular gravitational potential. The plots in Figure **9** demonstrate a physically satisfactory trend of both g_{tt} and g_{rr} functions.

Finally, the triplet of physical matter parameters (ρ, p_r, p_t) in the form of Eqs.(38) and (43) are

$$\rho = \frac{6r^4 + r^2(2x+7y) + 3y(x+y)}{8\pi x(2r^2+y)^2}, \tag{44}$$

$$\begin{aligned} p_r = & \Bigg[8\pi x \mathrm{h}_2^{3/2}\left(\frac{2r^2+y}{\mathrm{h}_2}\right)^{3/2}\sqrt{\frac{\mathrm{h}_1}{\mathrm{h}_2}}\Bigg\{D_2\mathrm{h}_2\sqrt{\mathrm{h}_1(2r^2+y)} + D_1\{\mathrm{h}_1(2r^2+y) \\ & \times\sqrt{\mathrm{h}_2} + \sqrt{y}\sqrt{\frac{2r^2+y}{\mathrm{h}_2}}\mathrm{h}_2^2\sqrt{\frac{\mathrm{h}_1}{\mathrm{h}_2}}\mathrm{h}_3\}\Bigg\}\Bigg]^{-1}\Bigg[D_1(x-r^2)(2r^2+y)\Bigg\{\mathrm{h}_2\sqrt{\frac{2r^2+y}{\mathrm{h}_2}} \\ & \times\sqrt{\frac{\mathrm{h}_1}{\mathrm{h}_2}}(3r^2+x+3y) + \sqrt{y}\sqrt{\mathrm{h}_2}(\mathrm{h}_2+x)\mathrm{h}_3\Bigg\} - D_2\sqrt{\mathrm{h}_1}\mathrm{h}_2^{3/2}\sqrt{2\mathrm{h}_2}\sqrt{\frac{2r^2+y}{\mathrm{h}_2}} \\ & \times\sqrt{\frac{\mathrm{h}_1}{\mathrm{h}_2}}\mathrm{h}_2 + x\Bigg], \end{aligned} \tag{45}$$

$$\begin{aligned} p_t = & \Bigg[8\pi x \mathrm{h}_2^{5/2}\left(\frac{2r^2+y}{\mathrm{h}_2}\right)^{5/2}\sqrt{\frac{\mathrm{h}_1}{\mathrm{h}_2}}\Bigg\{D_2\sqrt{\mathrm{h}_1}\mathrm{h}_2\sqrt{2r^2+y} + D_1\{\mathrm{h}_1(2r^2+y) \\ & \times\sqrt{\mathrm{h}_2} + \sqrt{y}\sqrt{\frac{2r^2+y}{\mathrm{h}_2}}\mathrm{h}_2^2\sqrt{\frac{\mathrm{h}_1}{\mathrm{h}_2}}\mathrm{h}_3\}\Bigg\}\Bigg]^{-1}\Bigg[D_1(x-r^2)(2r^2+y)\Bigg\{\mathrm{h}_2\sqrt{\frac{2r^2+y}{\mathrm{h}_2}} \end{aligned}$$

$$\times \sqrt{\frac{\mathrm{h}_1}{\mathrm{h}_2}}\{6r^4+8r^2y+y(x+3y)\}+\sqrt{y}\sqrt{\mathrm{h}_2}\{2r^4+2r^2y+y(x+y)\}\mathrm{h}_3\Big\}$$
$$-D_2\sqrt{\mathrm{h}_1}(\mathrm{h}_2)^{3/2}\sqrt{2r^2+y}\sqrt{\frac{2r^2+y}{\mathrm{h}_2}}\sqrt{\frac{\mathrm{h}_1}{\mathrm{h}_2}}\{2r^4+2r^2y+y(x+y)\}\Big]. \quad (46)$$

It is observed that the above field equations contain three constants that must be calculated via junction conditions. We already discussed that the exterior geometry in this context is considered as the the Schwarzschild metric (29). Matching our interior model with this exterior spacetime under the first fundamental form gives

$$\frac{D_1\sqrt{\frac{\mathrm{h}_1^*}{\mathrm{h}_2^*}}\{\sqrt{\mathrm{h}_2^*}(2R^2+y)\sqrt{\frac{\mathrm{h}_1^*}{\mathrm{h}_2^*}}+\mathrm{h}_2^*\sqrt{y}\sqrt{\frac{2R^2+y}{\mathrm{h}_2^*}}\mathrm{h}_3^*}{\sqrt{\mathrm{h}_1^*(2R^2+y)}}+D_2 = \sqrt{1-\frac{2\mathrm{M}}{R}}, \quad (47)$$
$$\frac{x(2R^2+y)}{(x-R^2)(R^2+y)} = 1-\frac{2\mathrm{M}}{R}, \quad (48)$$

where $\mathrm{h}_1^* = \mathrm{h}_1(R)$, $\mathrm{h}_2^* = \mathrm{h}_2(R)$, and $\mathrm{h}_3^* = \mathrm{h}_2(R)$. Moreover, the radial pressure is found to vanish at a specific value of r, which results after merging with Eq.(45) as

$$p_r(R) = 2D_1\mathrm{h}_2^*(x-R^2)2\mathrm{h}_2^*\Big\{\mathrm{h}_2^*\sqrt{\frac{2R^2+y}{\mathrm{h}_2^*}}\sqrt{\frac{\mathrm{h}_1^*}{\mathrm{h}_2^*}}(3R^2+x+3y)$$
$$+\sqrt{y}\mathrm{h}_2^{*3/2}+x\mathrm{h}_3^*\Big\}-D_2\mathrm{h}_2^{*3/2}\sqrt{2\mathrm{h}_1^*\mathrm{h}_2^*}\sqrt{\frac{2\mathrm{h}_2^*}{\mathrm{h}_2^*}}\sqrt{\frac{\mathrm{h}_1^*}{\mathrm{h}_2^*}}(\mathrm{h}_2^*+x)=0. \quad (49)$$

The simultaneous solution of Eqs.(47)-(49) gives the three constants as follows

$$x = \frac{R^3(R^2+y)}{4\mathrm{M}R^2+2\mathrm{M}y-R^3}, \quad (50)$$
$$D_1 = -\frac{\sqrt{1-\frac{2\mathrm{M}}{R}}(\mathrm{h}_2^*+x)}{2\sqrt{2yR^2\mathrm{h}_1^*\mathrm{h}_2^*}}, \quad (51)$$
$$D_2 = \frac{1}{4yR^2\mathrm{h}_1^*\mathrm{h}_2^*}\sqrt{1-\frac{2\mathrm{M}}{R}}\Big\{2yR^2\mathrm{h}_1^*(3R^2+x+3y)$$
$$+\sqrt{y}\mathrm{h}_2^{*3/2}\sqrt{\frac{R^2}{\mathrm{h}_2^*}+1}\sqrt{\frac{\mathrm{h}_1^*}{\mathrm{h}_2^*}}(\mathrm{h}_2^*+x)h_3^*\Big\}. \quad (52)$$

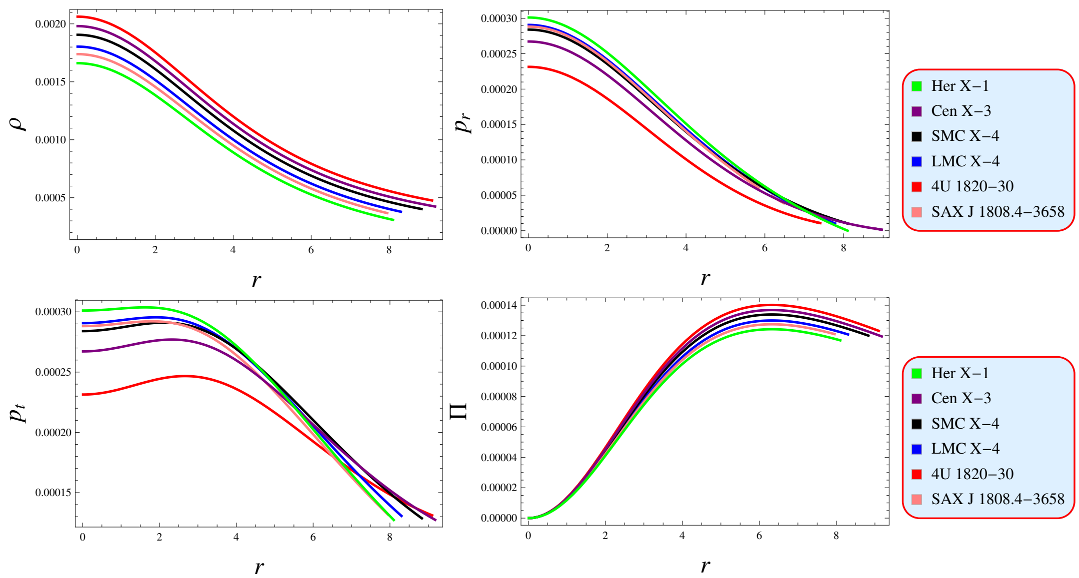

Figure 10: Fluid parameters for $y = 30$ corresponding to model II.

The matter triplet (44)-(46) and its physical properties are now graphically investigated. The profile of the pressure components, energy density and anisotropic factor is shown in Figure **10**. We also observe the vanishing of the radial pressure at the interface. At the center, $p_r(0) = constant = p{+}t(0)$, implying that the radial and tangential pressures are equal, resulting in the vanishing anisotropy at that point. Additionally, Figure **11** plots the regularity criteria for the above matter variables, showing a required trend.

Table 3: Various physical factors for different stars corresponding to model II.

Stars	ρ_c(**gm/cm^3**)	ρ_s(**gm/cm^3**)	p_c(**dyne/cm^2**)
$\mathrm{HerX-1}$	2.2181×10^{15}	3.9439×10^{14}	3.6024×10^{35}
$\mathrm{CenX-3}$	2.6422×10^{15}	5.5788×10^{14}	3.1960×10^{35}
$\mathrm{SMCX-4}$	2.5379×10^{15}	5.2457×10^{14}	3.4089×10^{35}
$\mathrm{LMCX-4}$	2.4028×10^{15}	4.8577×10^{14}	3.4870×10^{35}
$\mathrm{4U1820-30}$	2.7479×10^{15}	6.3320×10^{14}	2.7692×10^{35}
$\mathrm{SAXJ1808.4-3658}$	2.3091×10^{15}	4.7172×10^{14}	3.4461×10^{35}

Table **3** presents the central density, surface density and central pressure for all the considered starts under our model II. We notice that their values lie within the acceptable ranges which ultimately points the existence of

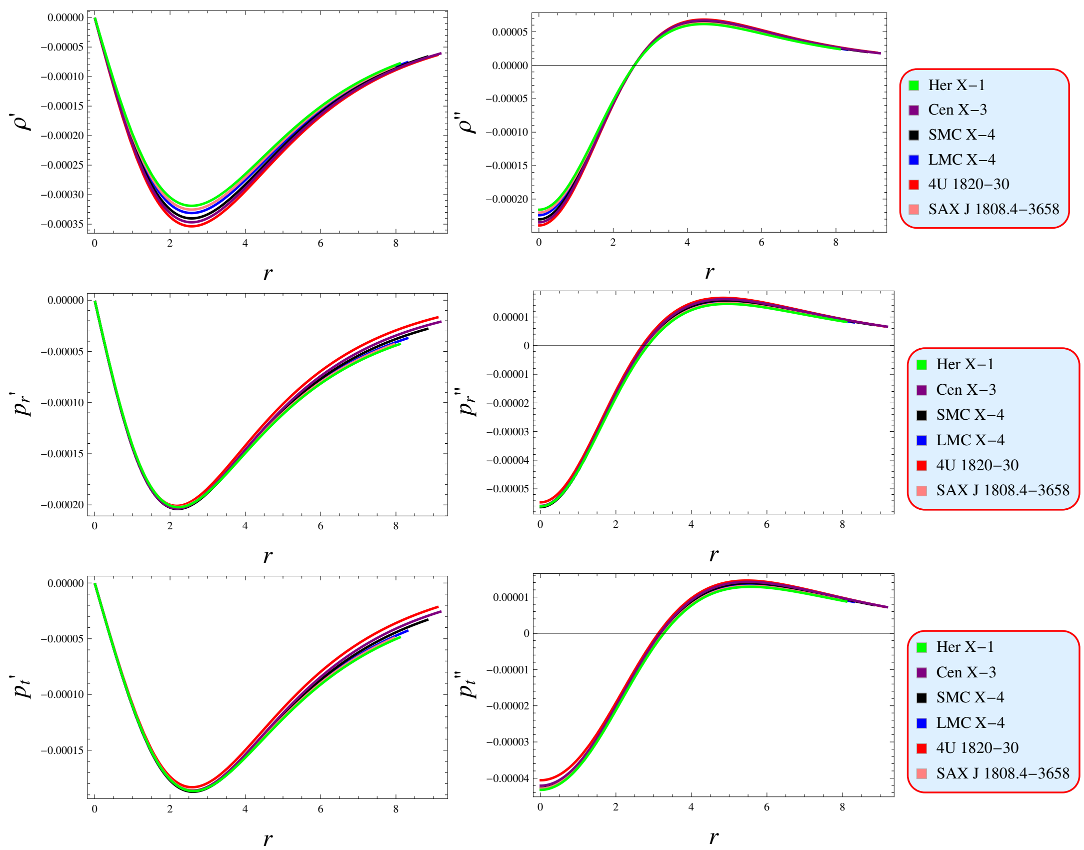

Figure 11: Regularity conditions for $y = 30$ corresponding to model II.

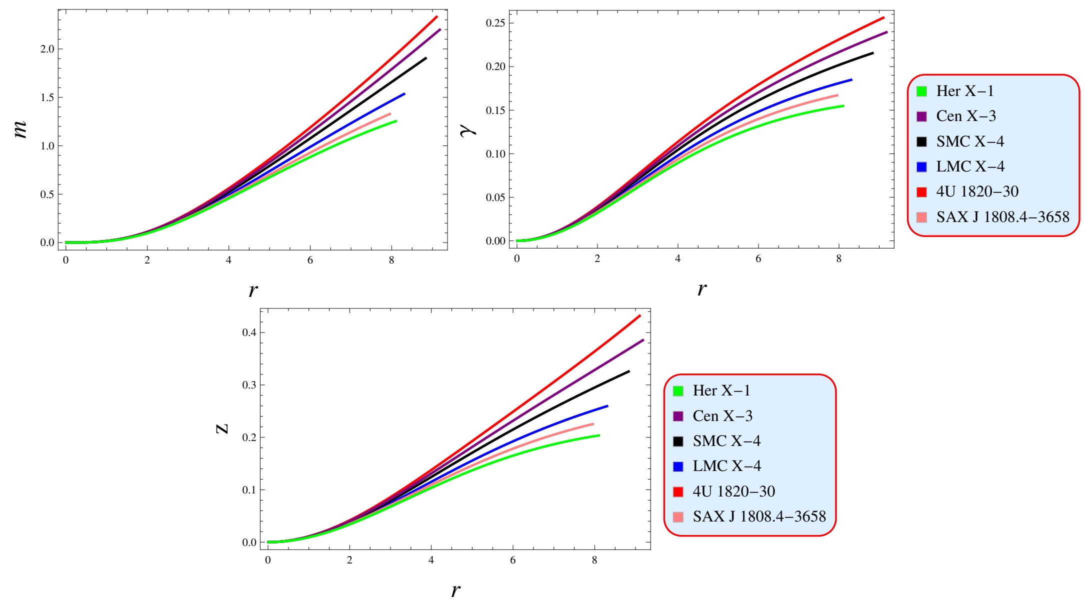

Figure 12: Physical factors for $y = 30$ corresponding to model II.

dense astrophysical objects. The mass function, redshift, and compactness factors are shown in Figure **12**, from which we see that the values of mass corresponding to all the considered stars are consistent with their observed masses. The behavior of the equation of state parameters is illustrated in Figure **13** that confirms the physical validity of our model II. We display only the trace and dominant energy constraints in Figure **14** which suggests that the suggested solution is viable and thus the corresponding interior contains the ordinary fluid. The net sum of all forces is found to be zero in Figure **15**, hence, the model II is in the state of equilibrium. We further analyze the stability in the same Figure using cracking and sound speed criteria, which confirms the stability of model II over the whole interior. The stability analysis is also performed through the adiabatic index in Figure **16**, and we observe the required results which are consistent with the earlier two tests.

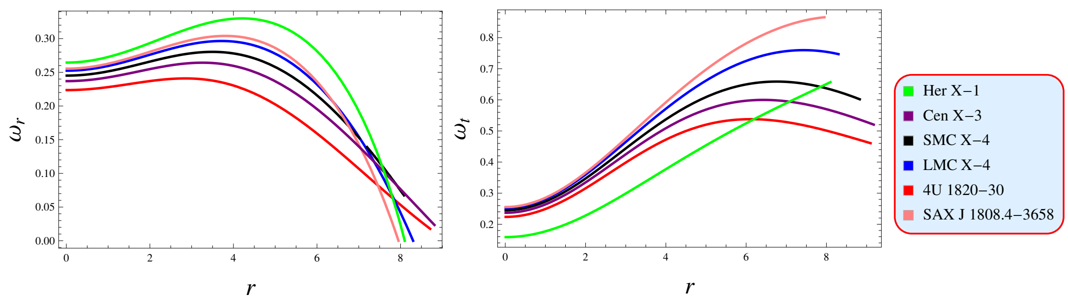

Figure 13: Equation of state parameters for $y = 30$ corresponding to model II.

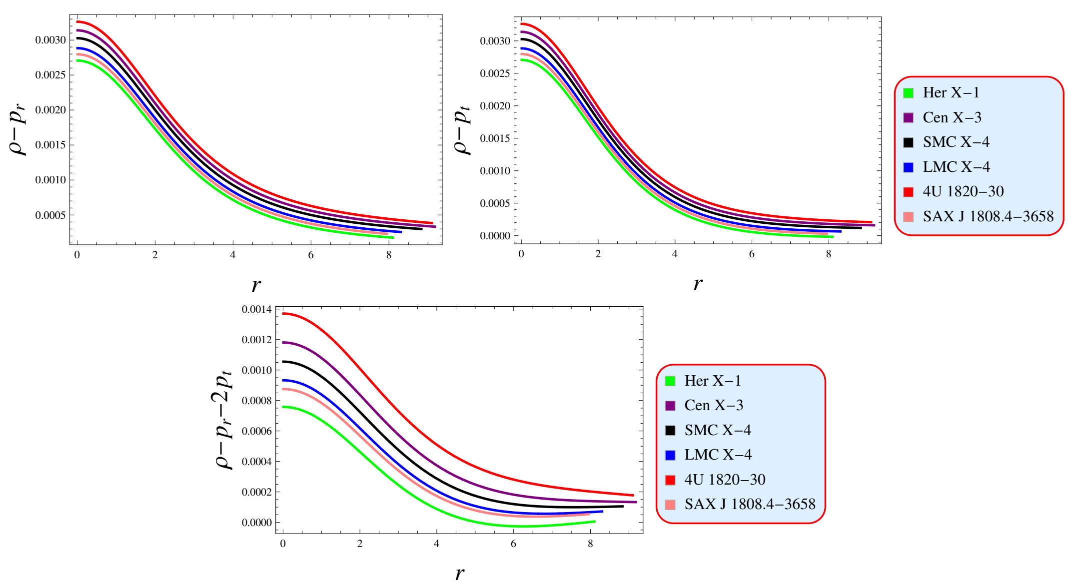

Figure 14: Energy bounds for $y = 30$ corresponding to model II.

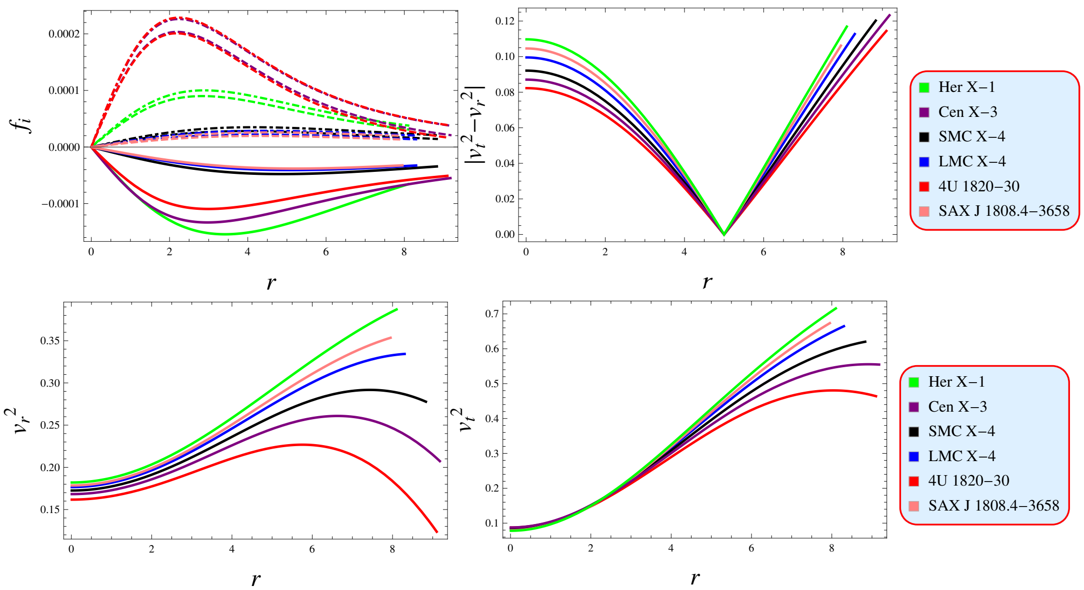

Figure 15: Equilibrium of forces, cracking, and sound speeds for $y = 30$ corresponding to model II.

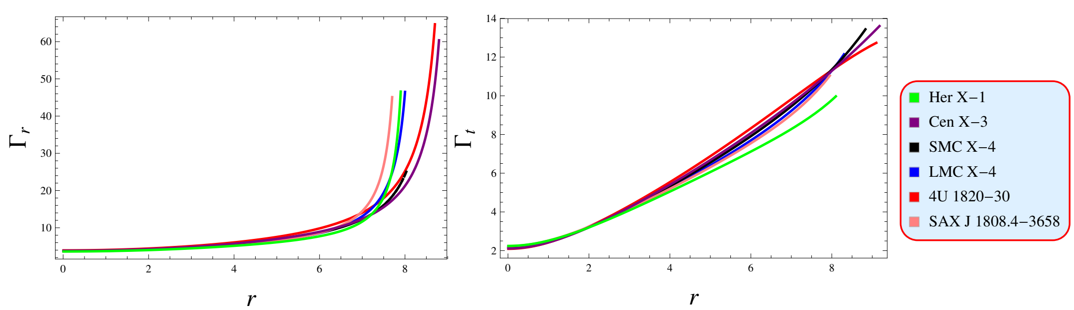

Figure 16: Adiabatic index for $y = 30$ corresponding to model II.

5 Conclusions

Two novel singularity-free anisotropic solutions are developed in this study through the utilization of different constraints. To achieve this, we have taken a static spherical interior spacetime and the corresponding governing field equations as well as the gravitational mass function have been constructed. Given that the system was under-determined, specific constraints have been introduced to obtain exact analytical solutions. We have considered certain types of g_{rr} metric potential and merged it with the anisotropy which resulted in differential equations of second-order involving the g_{tt} function. The temporal metric functions have then been determined by assuming particular types of the anisotropies (null in the core and increasing outwards), which results in our models I and II. At the spherical boundary, the constants associated with these metric functions have been derived by matching the interior and the external Schwarzschild spacetimes. Below is the detailed summary of the graphical analysis conducted for both our models for six distinct compact stars (Table **1**).

- We have determined that the metric functions and related matter determinants of both our models show the an appropriate profile which is required for the physical existence of stellar models (Figures **1, 2, 9** and **10**). At the spherical boundary, the radial pressures (27) and (45) reduce to zero which is also consistent with the second fundamental form of the boundary conditions. Tables **2** and **3** present the numerically computed values of these fluid parameters which lie in the acceptable range for stars to exist both theoretical and physical point of view.

- The anisotropy shows an increasing trend in both models that suggests a repulsive effect. Hence, our models remain stable for a long period of time. Additionally, the regularity conditions are also satisfied, as illustrated in Figures **3** and **11**. The results for the redshift, compactness, and mass functions are plotted in Figures **4** and **12** for models I and II, respectively. We observe that their profiles are consistent with the observations.

- Figures **5** and **13** clearly demonstrate that both parameters ω_r and ω_t are less than one that confirm the validity of our models. The physical viability of both resulting models is checked in Figures **6** and **14**, where the corresponding energy bounds are fully satisfied which ultimately supports the presence of normal fluid within the resulting interiors.

- The balance of all the forces acting on a self-gravitating bodies is also important to be checked. We have performed this analysis in Figures **7** and **15**, and deduced the hydrostatic equilibrium of our models as the sum of all the acting forces nullifies. In the same Figure, we have used two different tests, sound speed fluctuations and cracking criteria, to explore the stability. We have found that both criteria are fulfilled, claiming models I and II to be stable. Moreover, the adiabatic index is checked that also supports the stability (Figures **8** and **16**).

- It is concluded that both of our models satisfy a family of stability requirements and physical characteristics necessary for celestial bodies' existence in any gravitational theory. We, therefore, claim that the developed results are effective for modeling compact interiors coupled with the anisotropic fluid distribution.

The implications of this study extend to both theoretical and observational astrophysics. Theoretically, it reinforces the necessity of incorporating anisotropy in modeling compact stars, as isotropic assumptions often fail to capture the complex dynamics of high-density matter. Observationally, the models align with empirical data from known compact stars, offering a framework to interpret their mass-radius relationships and internal structures. Future work could explore the inclusion of more sophisticated equations of state, magnetic fields, or rotational effects to further refine these models. Additionally, extending this analysis to modified gravity theories or higher-dimensional spacetimes may uncover new phenomena in extreme gravitational environments. Ultimately, this study lays a solid foundation for future investigations into the enigmatic nature of compact objects and their role in the cosmos.

Data Availability Statement: No new data is generated in this study.

References

[1] K. Schwarzschild, Sitz. Deut. Akad. Wiss Berlin Kl. Math. Phys. **1916**, 189 (1916)

[2] K. Schwarzschild, Sitz. Deut. Akad. Wiss Berlin Kl. Math. Phys. **24**, 424 (1916)

[3] L. Herrera, N.O. Santos, Phys. Rep. **286**, 53 (1997)

[4] J. Ovalle, Phys. Rev. D **95**, 104019 (2017)

[5] J. Ovalle, R. Casadio, R. da Rocha, A. Sotomayor, Eur. Phys. J. C **78**, 122 (2018)

[6] T. Naseer, Phys. Dark Universe **46**, 101663 (2024)

[7] T. Naseer, M. Sharif, S. Manzoor, A. Fatima, Mod. Phys. Lett. A **39**, 2450048 (2024)

[8] J. Ospino, L.A. Nunez, Eur. Phys. J. C **80**, 166 (2020)

[9] B.V. Ivanov, Eur. Phys. J. C **81**, 227 (2021)

[10] Y. Feng et al., Chin. J. Phys. **90**, 372-386 (2024)

[11] T. Naseer, J.L. Said, Eur. Phys. J. C **84**, 808 (2024)

[12] L. Herrera, A. Di Prisco, J. Ospino, E. Fuenmayor, J. Math. Phys. **42**, 2129 (2001)

[13] W. Baade, F. Zwicky, Phys. Rev. **46**, 76 (1934)

[14] J. Jeans, Mon. Not. R. Astron. Soc. **82**, 122 (1922)

[15] G. Lemaitre, Ann. Soc. Sci. Brux. A **53**, 51 (1933)

[16] M. Ruderman, Annu. Rev. Astron. Astrophys. **10**, 427 (1972)

[17] R.F. Sawyer, Phys. Rev. Lett. **29**, 382 (1972)

[18] S.S. Yazadjiev, Phys. Rev. D **85**, 044030 (2012)

[19] C.Y. Cardall, M. Prakash, J.M. Lattimer, Astrophys. J. **554**, 322 (2001)

[20] R. Ciolfi, V. Ferrari, L. Gualtieri, Mon. Not. R. Astron. Soc. **406**, 2540 (2010)

[21] J. Frieben, L. Rezzolla, Mon. Not. R. Astron. Soc. **427**, 3406 (2012)

[22] V. Canuto, Annu. Rev. Astron. Astrophys. **12**, 167 (1974)

[23] H. Heiselberg, M. Hjorth-Jensen, Phys. Rep. **328**, 237 (2000)

[24] R.L. Bowers, E.P.T. Liang, Astrophys. J. **188**, 657 (1974)

[25] Z. Roupas, Astrophys. Space Sci. **366**, 9 (2021)

[26] D. Deb, B. Mukhopadhyay, F. Weber, Astrophys. J. **922**, 149 (2021)

[27] L. Herrera, J. Ospino, A. Di Prisco, Phys. Rev. D **77**, 027502 (2008)

[28] L. Herrera, W. Barreto, Phys. Rev. D **88**, 084022 (2013)

[29] S. Das, B.K. Parida, S. Ray, S.K. Pal, Phys. Sci. Forum **2**, 29 (2021)

[30] K. Lake, Phys. Rev. D **80**, 064039 (2009)

[31] L. Herrera, N.O. Santos, Phys. Rep. **286**, 53 (1997)

[32] L. Herrera, Phys. Rev. D **101**, 104024 (2020)

[33] M.K. Gokhroo, A.L. Mehra, Gen. Relativ. Gravit. **26**, 75 (1994)

[34] N. Pant, R.N. Mehta, M. Pant, Astrophys. Space Sci. **332**, 473 (2011)

[35] Y.K. Gupta, S.K. Maurya, Astrophys. Space Sci. **332**, 155 (2011)

[36] A. Rehman et al., Nucl. Phys. B **1013**, 116852 (2025)

[37] S.K. Maurya, Y.K. Gupta, S. Ray, B. Dayanandan, Eur. Phys. J. C **75**, 225 (2015)

[38] S.K. Maurya, A. Banerjee, S. Hansraj, Phys. Rev. D **97**, 044022 (2018)

[39] S.K. Maurya, S.D. Maharaj, J. Kumar, A.K. Prasad, Gen. Relativ. Gravit. **51**, 86 (2019)

[40] A. Rehman et al., Nucl. Phys. B **1015**, 116897 (2025)

[41] M.F. Shamir, G. Mustafa, Q. Hanif, Int. J. Mod. Phys. A **35**, 2050083 (2020)

[42] K. Hassan et al., Chin. J. Phys. **91**, 916 (2024)

[43] B. Siza et al., Eur. Phys. J. C **84**, 1203 (2024)

[44] T. Naseer, Chin. J. Phys. **96**, 1212-1231 (2025)

[45] M. Al Hadhrami et al., Pramana **97**, 13 (2022)

[46] S.K. Maurya et al., Mon. Not. R. Astron. Soc. **519**, 4303 (2023)

[47] T. Naseer, Eur. Phys. J. C **84**, 1256 (2024)

[48] L. Baskey, S. Ray, S. Das, S. Majumder, A. Das, Eur. Phys. J. C **83**, 307 (2023)

[49] M. Sharif, T. Naseer, Int. J. Mod. Phys. D **31**, 2240017 (2022)

[50] M. Sharif, Q. Ama-Tul-Mughani, Chin. J. Phys. **65**, 207 (2020)

[51] T. Naseer, Astropart. Phys. **166**, 103073 (2025)

[52] S. Sarkar, N. Sarkar, P. Rudra, F. Rahaman, T. Ghorui, Eur. Phys. J. C **83**, 1005 (2023)

[53] E. Demir, et al., Chin. J. Phys. **91**, 299 (2024)

[54] C.W. Misner, D.H. Sharp, Phys. Rev. **136**, B571 (1964)

[55] M.S.R. Delgaty, K. Lake, Comput. Phys. Commun. **115**, 395 (1998)

[56] T. Naseer, Ann. Phys. **479**, 170035 (2025)

[57] H.A. Buchdahl, Phys. Rev. **116**, 1027 (1959)

[58] B.V. Ivanov, Phys. Rev. D **65**, 104011 (2002)

[59] R.C. Tolman, Phys. Rev. **55**, 364 (1939)

[60] J.R. Oppenheimer, G.M. Volkoff, Phys. Rev. **55**, 374 (1939)

[61] H. Abreu, H. Hernandez, L.A. Nunez, Class. Quantum Grav. **24**, 4631 (2007)

[62] L. Herrera, Phys. Lett. A **165**, 206 (1992)

[63] H. Heintzmann, W. Hillebrandt, Astron. Astrophys. **38**, 51 (1975)

[64] M. Kohler, K.L. Chao, Z. Naturforsch. A **20**, 1537 (1965)

[65] R.S. Tikekar, Curr. Sci. **39**, 460 (1970)